Nonlinear Equilibration of Two-Dimensional Eady Waves

NOBORU NAKAMURA

Program in Atmospheric and Oceanic Sciences, Princeton University, Princeton, New Jersey

ISAAC M. HELD

Geophysical Fluid Dynamics Laboratory/NOAA, Princeton University, Princeton, New Jersey

(Manuscript received 5 December 1988, in final form 11 May 1989)

ABSTRACT

The initial-value problem for Eady's model is reexamined using a two-dimensional (x–z) primitive equation model. It is generally accepted that a finite amplitude instability of Eady's basic state will produce a frontal discontinuity in a finite time. When diffusion prevents the frontal discontinuity from forming, the wave amplitude eventually stops growing and begins to oscillate. We analyze this equilibration and suggest that it is a result of enhanced potential vorticity in the frontal region that is mixed into the interior from the boundaries. The dynamics of equilibration is crudely captured in a modified quasi-geostrophic model in which the zonal-mean static stability is allowed to vary. The magnitude of the meridional wind speed of the equilibrated wave is $O(N_0H)$, where N_0 is the initial buoyancy frequency and H is the depth of the fluid. This is of the same order as the amplitude of the wave predicted by semigeostrophic theory at the point of frontal collapse. Scaling arguments are presented to determine the three-dimensional flows for which this equilibration mechanism should be important. It is argued that this mechanism is likely to be of some importance for shallow cyclones forming in regions of weak low-level static stability.

1. Introduction

The nonlinear development of baroclinic instabilities has been studied from a wide variety of perspectives since the pioneering work on the linear theory by Charney (1947) and Eady (1949). Most of this work can be categorized as focusing either on frontogenesis or on the equilibration of the large-scale disturbance. Frontogenesis can be studied in the context of a developing disturbance, without regard to the processes of equilibration, as in the numerical integration by Williams (1967) of two-dimensional Eady wave instability, and in the elegant semigeostrophic theory of Hoskins and Bretherton (1972). The theory of the latter paper shows that the unstable Eady wave grows exponentially with no hint of equilibration, up to the point of frontal collapse.

In studies of wave equilibration, on the other hand, often little reference is made to frontogenesis. This is certainly the case in weakly nonlinear theories in which the change in shape of the linearly unstable modes is small; but even in strongly nonlinear modeling studies conducted with the quasi-geostrophic equations, no true frontal discontinuities can be formed in finite times, as the advection of relative vorticity by the cross frontal circulation is ignored. Life cycle studies using the primitive equations on the sphere, as in Simmons and Hoskins (1978), are capable of simultaneously producing realistic frontogenesis and equilibration. Comparisons of these primitive equation calculations with simpler quasi-geostrophic models suggest that the simpler models without well-defined fronts are indeed adequate for simulating the equilibration of large-scale disturbances.

In this study we analyze a two-dimensional model (in x and z) that both equilibrates and produces a front, so as to examine the interplay between these two processes in a simpler context. A vertically sheared zonal flow is perturbed with a disturbance that is independent of y (latitude) and the finite amplitude evolution is followed through the frontal formation stage. This two-dimensional model is a very special case; if quasi-geostrophic theory were valid the disturbance would not equilibrate at all; being independent of y, the disturbance cannot modify the meridional temperature gradient or vertical wind shear. While this two-dimensional evolution is not realistic for large-scale disturbances in the atmosphere, it is a case for which frontogenesis seems most likely to play some role in the equilibration.

Similar models have been studied by Arakawa (1962) and Orlanski (1986). Arakawa uses a balanced model and finds that the growth of the disturbance does cease, due to non-quasi-geostrophic effects. Of these effects, he argues that the increase in static stability

Corresponding author address: Dr. Noboru Nakamura, JISAO AK-40, University of Washington, Seattle, WA 98195.

of the zonally averaged flow is primarily responsible for the equilibration. Orlanski uses a higher resolution primitive equation model in which the disturbance develops a sharp frontal structure prior to leveling off. Orlanski suggests that the frontal dynamics itself plays a role in preventing the disturbance from continuing to grow.

Our goal in this paper is to clarify the mechanisms responsible for equilibration in two-dimensional models such as those of Arakawa and Orlanski. For this purpose we return to the classic initial-value problem for Eady's model, using the primitive equations. The only distinction between our model and that of Williams (1967) is the inclusion of diffusion to allow the integration to pass through the time of frontal collapse. The model is briefly described in section 2. The equilibration is analyzed in section 3. In section 4 we attempt to describe the conditions under which this kind of equilibration might be important for three-dimensional disturbances.

2. The initial-value Eady problem

The numerical model used in this study is a simplified version of the one described in Orlanski and Ross (1977), and those readers interested in the details of the model architecture may refer to that paper. The hydrostatic and Boussinesq approximations are made on an f-plane, consistent with the Eady problem. A basic state flow is assumed with uniform horizontal and vertical temperature gradient; the perturbation fields superposed on this mean flow are assumed independent of y. The set of equations we will be dealing with are the following:

$$\frac{d\zeta}{dt} = f\frac{\partial v}{\partial z} - \frac{g}{\theta_0}\frac{\partial \theta}{\partial x} + K_{HM}\frac{\partial^2 \zeta}{\partial x^2} + K_{VM}\frac{\partial^2 \zeta}{\partial z^2} \quad (1)$$

$$\frac{dv}{dt} + f(u - \bar{u}_g) = K_{HM}\frac{\partial^2 v}{\partial x^2} + K_{VM}\frac{\partial^2 v}{\partial z^2} \quad (2)$$

$$\frac{d\theta}{dt} + v\frac{\partial \bar{\theta}}{\partial y} = K_{HT}\frac{\partial^2 \theta}{\partial x^2} + K_{VT}\frac{\partial^2 \theta}{\partial z^2}, \quad (3)$$

where the circulation in the x–z plane is described in terms of a steamfunction Φ

$$u \equiv \frac{\partial \Phi}{\partial z}, \quad w \equiv -\frac{\partial \Phi}{\partial x}, \quad \zeta \equiv \frac{\partial u}{\partial z} = \frac{\partial^2 \Phi}{\partial z^2}, \quad (4)$$

$$\frac{g}{\theta_0}\frac{\partial \bar{\theta}}{\partial y} = -f\frac{\partial \bar{u}_g}{\partial z} \equiv -f\Lambda \quad \text{(time independent)}, \quad (5)$$

and

$$\frac{d}{dt} \equiv \frac{\partial}{\partial t} + \frac{\partial \Phi}{\partial z}\frac{\partial}{\partial x} - \frac{\partial \Phi}{\partial x}\frac{\partial}{\partial z}.$$

Orlanski and Ross use a stability-dependent viscosity; here we simply use constant coefficients. Rigid lid boundary conditions are applied at $z = 0$ and H. All variables are periodic in x, with the domain length L equal to the wavelength of the initial disturbance. To minimize diffusive effects at the boundaries, we assume that thermal wind balance holds at $z = 0$ and H, and that the static stability at the boundary remains equal to its initial value:

$$w = 0, \quad f\frac{\partial v}{\partial z} = \frac{g}{\theta_0}\frac{\partial \theta}{\partial x}, \quad f\frac{\partial u}{\partial z} = -\frac{g}{\theta_0}\frac{\partial \bar{\theta}}{\partial y} \equiv f\Lambda,$$

$$\frac{\partial}{\partial z}\theta(x, t) = \frac{\partial}{\partial z}\theta(x, 0) \quad \text{at} \quad z = 0, H. \quad (6)$$

Unless otherwise stated, the resolution is $\Delta z = H/20$ and $\Delta x = L/100$. We first describe the solution for the following choice of the model parameters:

$$H = 10 \text{ km}, \quad f = 10^{-4}\ \text{s}^{-1}, \quad \Lambda = 10^{-3}\ \text{s}^{-1},$$

$$N \equiv N_0 = 5 \times 10^{-3}\ \text{s}^{-1}, \quad K_{VT} = 5\ \text{m}^2\ \text{s}^{-1},$$

$$K_{HT} = 10^4\ \text{m}^2\ \text{s}^{-1}, \quad (K_{VM}, K_{HM}) = 0.7(K_{VT}, K_{HT}).$$

The corresponding Richardson number ($\text{Ri} = N_0^2/\Lambda^2$) is 25. The length of the domain L is set equal to 2000 km, which is very close to the most unstable wavelength in the quasi-geostrophic, large Ri limit. The initial condition is a small amplitude disturbance with the vertical structure of the (quasi-geostrophic) unstable mode.

The solid curve in Fig. 1 shows the time evolution of the maximum meridional wind speed $|v|_m$, which always occurs on the boundaries. Departures from exponential growth become evident near day 5. The amplitude peaks at nearly 90 m s^{-1} after day 7, after which it oscillates about a somewhat smaller value. The maximum rms velocity obtained is about 40 m s^{-1}. Figure 2 shows the evolution of the x–z structure of the velocity from day 4 to day 8. Up to day 5 one sees the continuous reduction in scale of the region of cyclonic vorticity along the boundaries, familiar from the work of Williams (1967), and Hoskins and Bretherton (1972). After day 5, diffusion becomes important in the frontal zones. In the absence of diffusion, the numerical model develops severe grid point noise shortly after day 5. Our result is similar to that of Gall et al. (1987) and Garner (1989) who study a front created by a deformation field, in that no minimum frontal scale appears in the absence of diffusion.

Shortly after the fronts are formed, significant changes in wave structure occur. The vertical tilt of the wave diminishes noticeably by day 7 and reverses by day 8. It is the change in sign of the associated baroclinic energy conversion that causes the wave amplitude to cease growing and then decay. We have confirmed this by comparing the baroclinic energy conversion (proportional to mean poleward heat flux) with the direct destruction of eddy potential and kinetic energy by diffusion. The latter is always an order of magnitude smaller than the former. The conversion of the mean

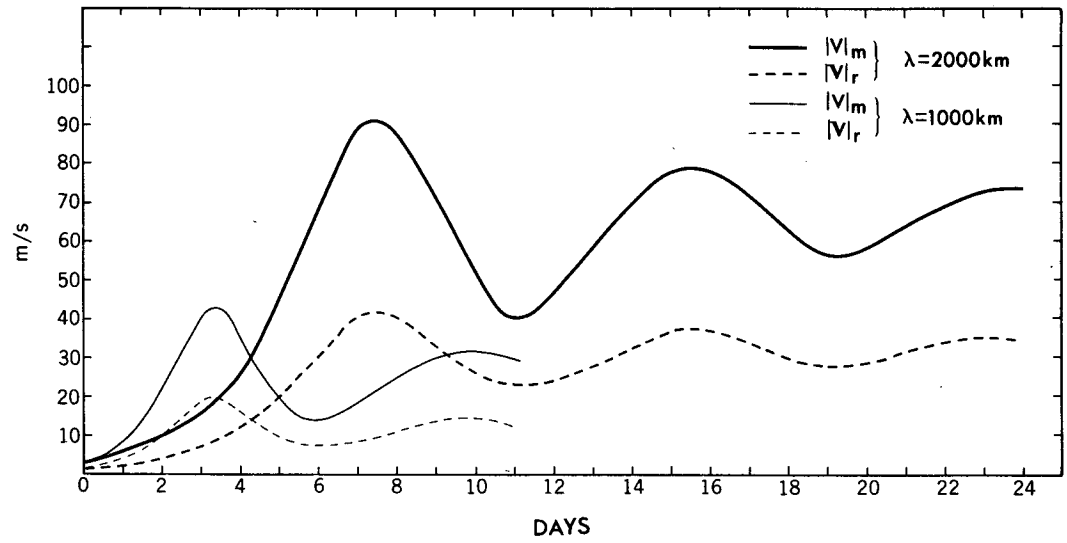

FIG. 1. Evolution of the maximum meridional wind speed $|v|_m$ (solid) and rms velocity of the wave $|\mathbf{v}|_r$ (domain average of $[(u-[u])^2+v^2]^{1/2}$, dashed). Thick solid curve: $|v|_m$ for the control run with initial wavelength $\lambda = 2000$ km, Ri = 25, and geostrophic shear $\Lambda = 10^{-3}\ s^{-1}$. Thick dashed curve: Same as solid curve but for $|\mathbf{v}|_r$. Thin solid curve: $|v|_m$ for the short-wave case: $\lambda = 1000$ km with one-fourth static stability N_0^2 (Ri = 6.25). Thick dashed curve: Same as solid curve but for $|\mathbf{v}|_r$.

state kinetic energy into the kinetic energy of the disturbance (proportional to the vertical flux of zonal momentum) is also negligible.

Figure 3 shows the changes in structure of the disturbance potential temperature field. The warm sector (the region warmer than the initial condition at that latitude and height) is stippled. After day 5 the disturbance begins to "occlude" as the warm sector ahead of the front is lifted off the surface. The vertical heat flux associated with this process increases the mean stability of the atmosphere dramatically. Figure 4 shows that the mean potential temperature difference between the top and bottom boundaries increases by nearly a factor of 6 as the wave reaches maximum amplitude and then oscillates about a value 3–4 times its initial value.

Although the diffusive terms appear negligible in the global energetics, the detailed evolution of the system does become sensitive to these terms as it passes through the frontal formation stage and the warm sector pinches off the surface. Figure 5 provides some examples of this sensitivity, corresponding to the choice of diffusion coefficient listed in Table 1. Figure 5a shows the evolution of $|v|_m$ for cases in which the vertical or horizontal momentum diffusion, or both, are increased by a factor of 4. Figure 5b shows analogous results for the thermal diffusion. The solutions begin to diverge near day 5 as the front forms. However, the sensitivity is sufficiently weak at first that the differences in diffusivity result in only small changes in the maximum amplitude obtained by the eddy. Increased horizontal momentum diffusion decreases this amplitude slightly; increased vertical momentum diffusion has little effect, while the horizontal and vertical thermal diffusion have small but compensating effects. The solutions in Fig. 5 do begin to differ dramatically after the decay of the initial disturbance. The period and the amplitude of the oscillations that develop in the control run in this latter state are evidently strongly dependent on the choice of diffusivity.

We have repeated the control run with twice the horizontal and vertical resolution. The very small differences produced would hardly be visible in Figs. 1–4. The calculations with larger diffusivities in Fig. 5 should be even less sensitive to the resolution.

Calculations have also been performed holding all parameters fixed as in the control run except for the initial static stability N_0. The result from one such integration, with the value of N_0 reduced by a factor of 2, has been included in Fig. 1. The wavelength of the initial disturbance, and the length of the channel have also been divided by 2 so that we are again dealing with a mode that is close to being the most unstable. The corresponding Richardson number is now 6.25. The amplitude attained by the disturbance is approximately half of that attained in the control, consistent with the dependence of amplitude on the wavelength of the disturbance found by Orlanski (1986). Calculations with other values of N_0 confirm that $|v|_m \propto N_0$, as displayed in Fig. 6.

If one nondimensionalizes horizontal, vertical and time scales by N_0H/f, H, and $f\Lambda/N_0$ respectively, the only nondimensional parameters that emerge are Ri and nondimensional measures of the diffusivities. Disregarding the latter based on the results in Fig. 5, we expect the functional dependence $|v|_m \propto \Lambda H$

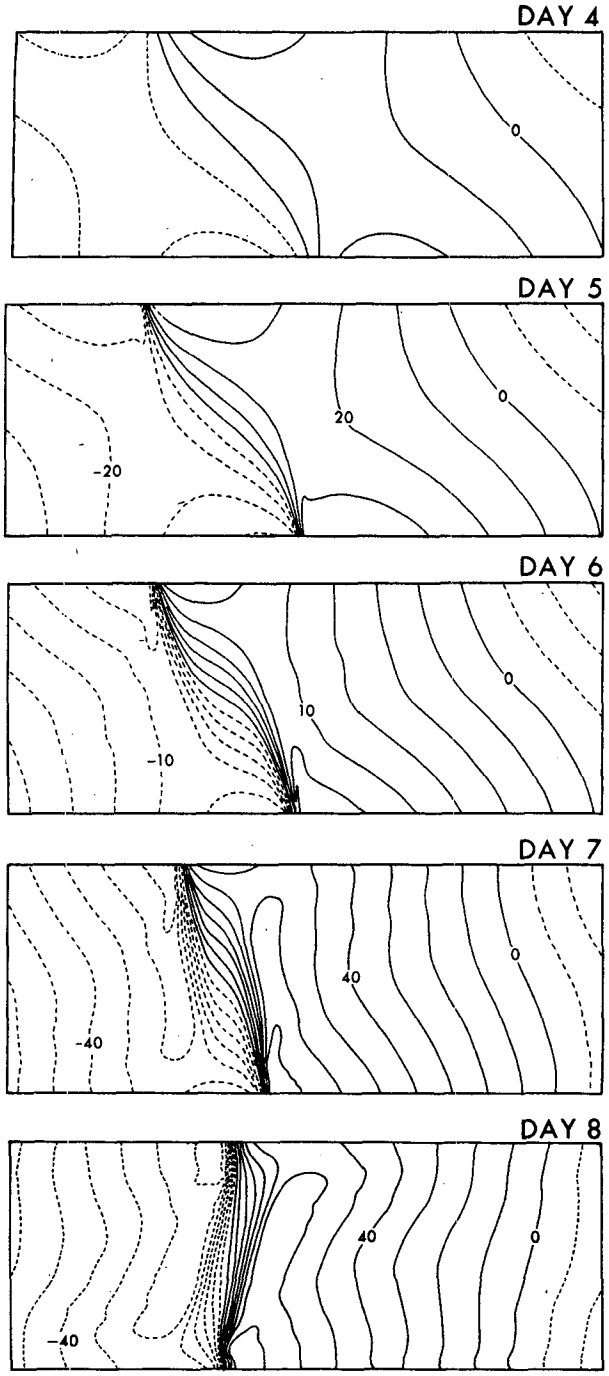

FIG. 2. Evolution of x–z structure of v-field for the control run. λ = 2000 km, Ri = 25. Contour interval is 10 m s^{-1}.

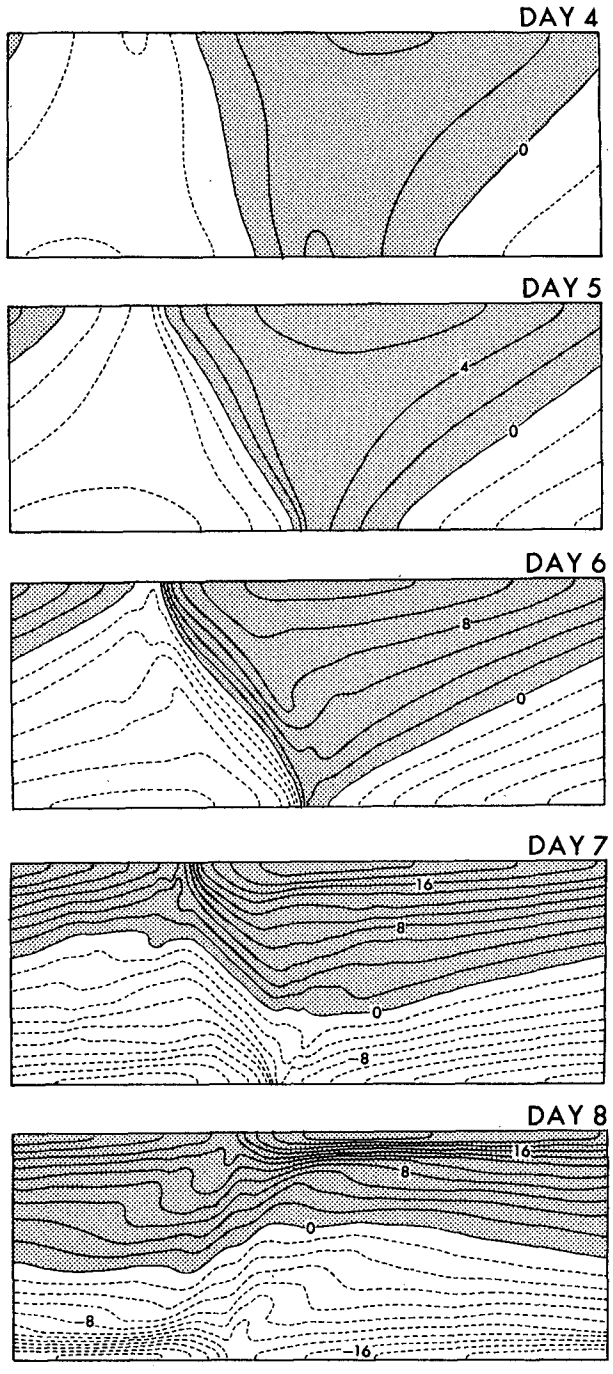

FIG. 3. Evolution of x–z structure of perturbation potential temperature field (deviation from the initial state) for the control run. Contour interval is 2 K.

$\times$ func(N_0/Λ). Given the approximate proportionality between $|v|_m$ and N_0, the implication is that $|v|_m$ is, to first approximation, independent of Λ.

3. Dynamics of the equilibration

The equilibration of the two-dimensional Eady wave cannot be understood on the basis of a standard quasi-geostrophic model. The exponentially growing normal mode with no y-dependence is an exact solution of the quasi-geostrophic equations, so the wave continues to grow indefinitely without changing its horizontal and vertical structure. The increase in static stability seen in Fig. 4 and the frontal formation itself, neither of

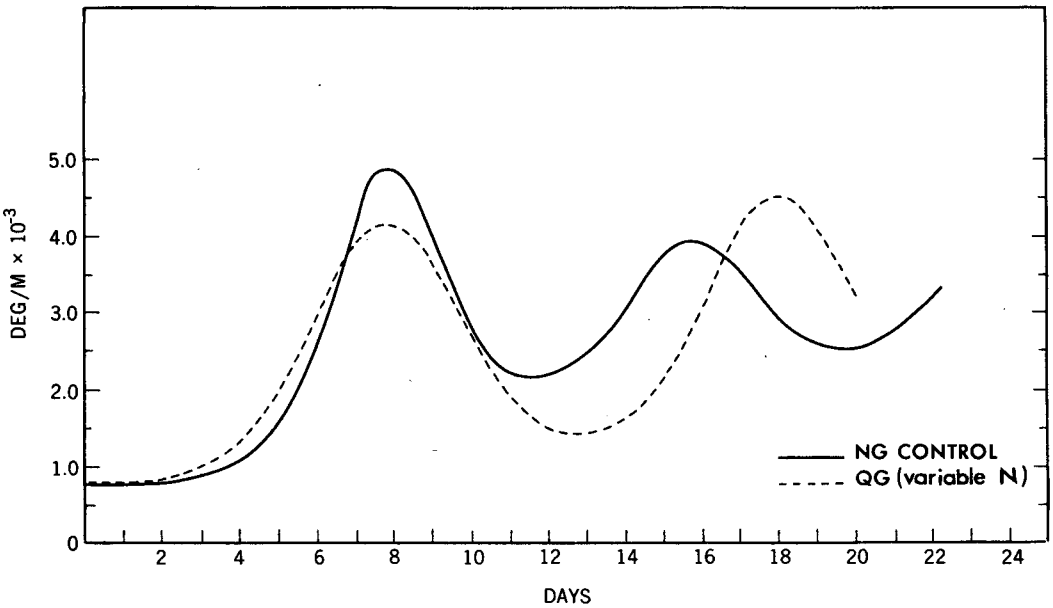

FIG. 4. Evolution of the domain-averaged lapse rate. Solid curve: Control (λ = 2000 km, Ri = 25). Dashed curve: Same initial condition but for quasi-geostrophic model with variable N^2 (see text).

which are present in the quasi-geostrophic (QG) solution, are the obvious candidates for equilibrating the wave.

Yet no hint of equilibration is seen in the semi-geostrophic Eady solution, which allows both the front to form and static stability to change. In the semi-geostrophic (SG) space defined by

$$T \equiv t, \quad X \equiv x + v_g/f, \quad Z \equiv z,$$

the geostrophic momentum approximation to the potential vorticity is related to the geostrophic streamfunction ψ by

$$q_g = \frac{f\theta_0}{g} \frac{\partial^2\psi/\partial Z^2}{f^2 - \partial^2\psi/\partial X^2}; \quad fv_g = \frac{\partial\psi}{\partial X}; \quad g\frac{\theta}{\theta_0} = \frac{\partial\psi}{\partial Z}.$$

For the perturbations, denoted by a prime,

$$\frac{\partial^2}{\partial X^2}\psi + \frac{f\theta_0}{gq_g}\frac{\partial^2}{\partial Z^2}\psi' = 0 \tag{12}$$

(Hoskins 1975). Since the potential vorticity is conserved and initially uniform

$$q_g = \frac{\theta_0}{fg}\frac{\partial^2\bar{\psi}}{\partial Z^2} = f(\theta_0/g)(N_0^2 - \Lambda^2),$$

it remains uniform for all times. Therefore, (12) becomes identical to the QG potential vorticity equation for the Eady problem in the limit of large Richardson number. The potential vorticity in the SG problem plays the role of the static stability in the QG problem. With the boundary conditions being also of an identical form, the two systems yield the same growth rate. In the SG solution, frontal collapse occurs in physical space when the coordinate transformation becomes singular, i.e., when the vorticity predicted in SG space, v_g/L, where L is the initial length scale of the disturbance, approaches f, or

$$v_g \approx fL \approx N_0 H. \tag{13}$$

This gives the amplitude of the baroclinic disturbance at the point of frontal collapse.

The inviscid SG model fails to explain the equilibration that appears in the numerical solution. To change the growth rate in the SG model for a fixed wavelength and vertical shear, one must modify the potential vorticity q_g. This is impossible for adiabatic, inviscid dynamics wherein q_g is conserved and remains uniform. However, we argue below that diffusive processes included in (1)–(3) change the interior potential vorticity in such a way as to cause the disturbance to equilibrate.

Shown in Fig. 7 is Ertel potential vorticity (which is very close to q_g in this two-dimensional model) of the control run in the equilibrating stage. The potential vorticity (PV) is virtually uniform before the surface fronts are formed. Once the front is formed, large positive PV develops near the surface discontinuity and permeates into the interior of the flow, accompanied by regions of very weak negative values ahead of the front. By day 7, the entire frontal region is occupied by enhanced PV.

This increase in PV can then be thought of as stabilizing the flow just as an increase in static stability stabilizes a QG flow; the larger static stability causes

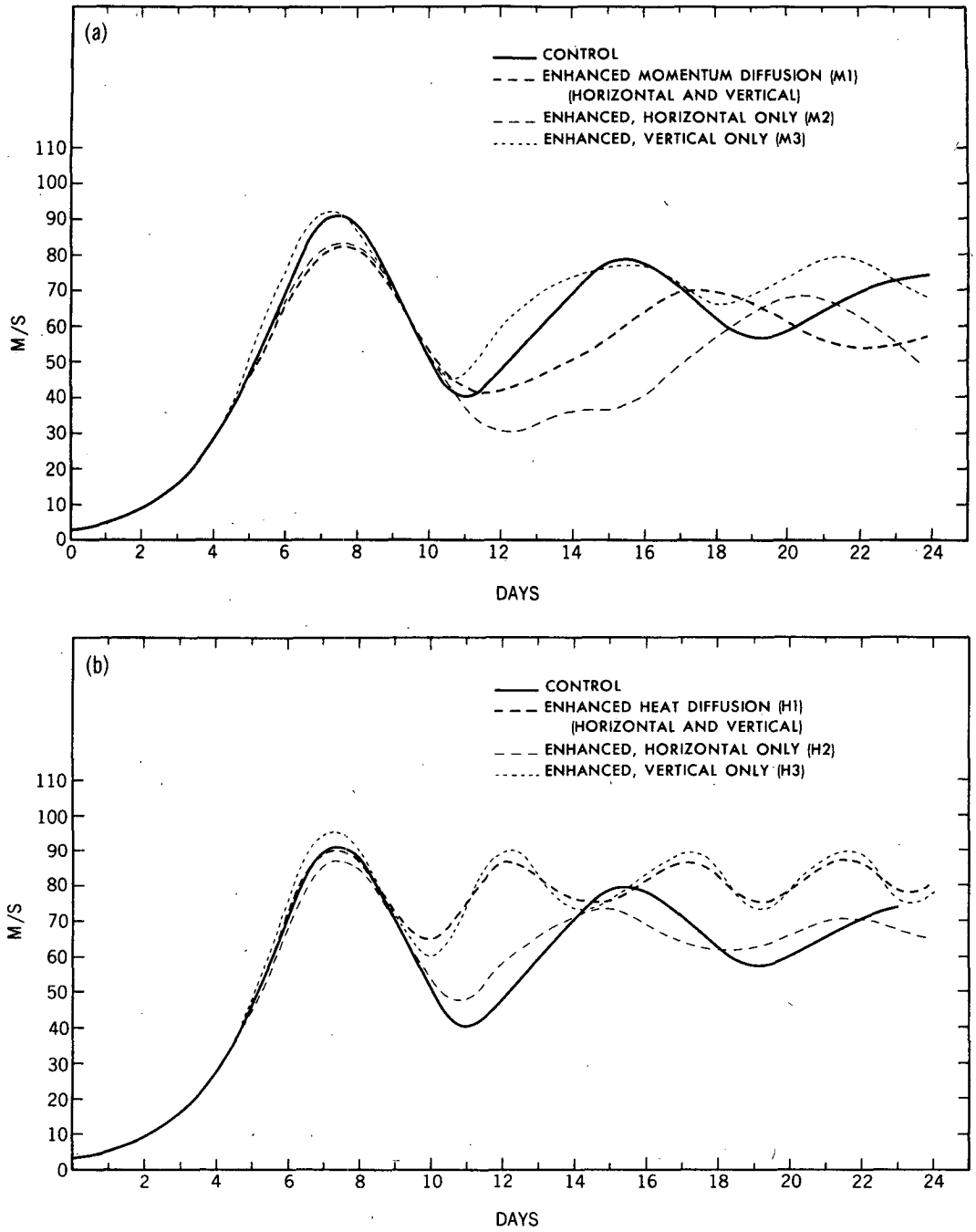

FIG. 5. (a) Evolution of maximum meridional wind speed $|v|_m$ with different combination of momentum diffusion (see Table 1). Solid curve: Control. Dashed curve: Both horizontal and vertical momentum diffusion are quadrupled from the control (M1). Thin dashed curve: Only horizontal momentum diffusion is quadrupled (M2). Dotted curve: Only vertical momentum diffusion is quadrupled (M3). (b) Same as (a) but with a different combination of heat diffusion. Solid curve: Control. Dashed curve: Both horizontal and vertical heat diffusion are quadrupled from the control (H1). Thin dashed curve: Only horizontal heat diffusion is quadrupled (H2). Dotted curve: Only vertical heat diffusion is quadrupled (H3).

the disturbance to become more strongly trapped at the boundaries, reducing the interaction between the two boundaries, and allowing the upper-level disturbance to be sheared past the low-level disturbance by the mean flow, therby reversing the baroclinic energy conversion. Alternatively, one can think of the increase in stability as shifting the short-wave cutoff for instability past the wavelength of the disturbance. Note also

TABLE 1. Combination of diffusion coefficients for the comparative runs in Fig. 5.

Cases	Momentum diffusion		Heat diffusion	
	K_{VM} ($m^2 s^{-1}$)	K_{HM} ($m^2 s^{-1}$)	K_{VT} ($m^2 s^{-1}$)	K_{HT} ($m^2 s^{-1}$)
Control	3.5	7000	5	10 000
M1	14	28 000	5	10 000
M2	3.5	28 000	5	10 000
M3	14	7000	5	10 000
H1	3.5	7000	20	40 000
H2	3.5	7000	5	40 000
H3	3.5	7000	20	10 000

that in SG space, the enhanced PV would occupy a larger fraction of the domain than in the x–z space of Fig. 7.

To understand the increase in PV, it is useful to think of the boundaries at $z = 0$ and H as being isentropic surfaces, introducing isentropic layers of infinitesimal thickness along the boundaries so that the correct temperature gradients exist interior to these layers. A sheet of PV is thereby created at each boundary, as discussed by Bretherton (1966) for the QG case. Since there can be no net creation or destruction of the PV contained within any two isentropic surfaces (Haynes and McIntyre 1987), one should think of the source of the high PV air in Fig. 7 as these boundary reservoirs which, as the result of the diffusive mixing at the front, are lifted off the surface along with the surface air. Figure 8 schematically illustrates this process.

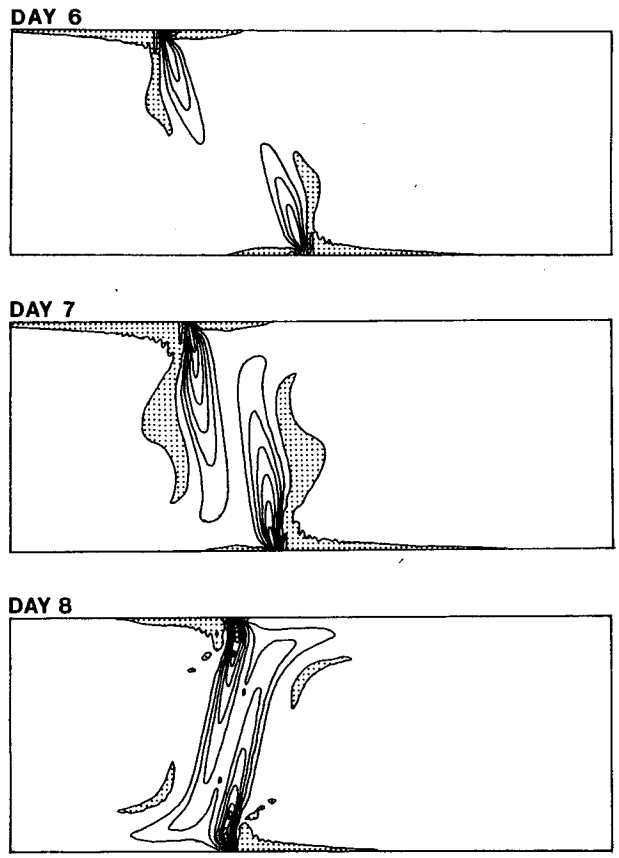

FIG. 7. Evolution of Ertel potential vorticity. Contour interval is 10^{-7} K m^{-1} s^{-1}. Negative regions are stippled. The field is initially uniform and 7.7×10^{-8} K m^{-1} s^{-1}.

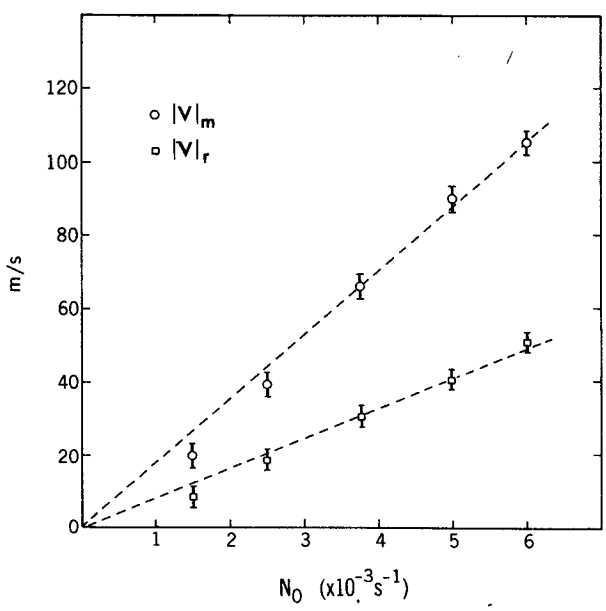

FIG. 6. Plot of $|v|_m$ and $|v|_r$ (same definition as in Fig. 1) as a function of N_0. Dashed lines are determined by the least mean square technique.

The details of this generation of high interior PV are complex, but using scaling arguments one can estimate the order of magnitude of the increase, averaged over

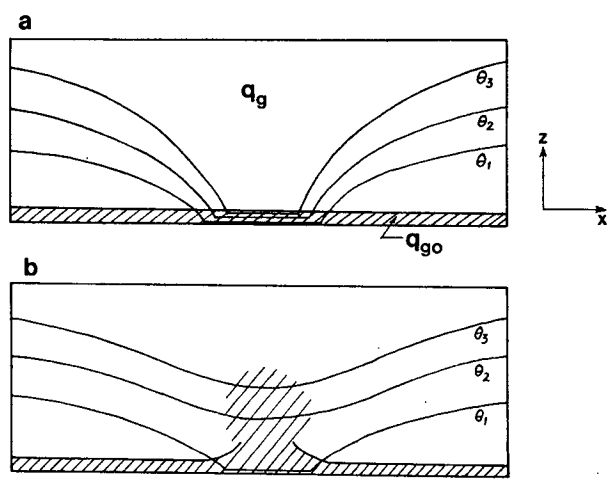

FIG. 8. Schematic view of escaping potential vorticity associated with the pinching-off of isentropes. (a) Before the front is formed, (b) after the front is formed. See text for explanation.

the domain. The magnitude of the potential temperature perturbation θ' along the surface at the point of frontal collapse can be obtained from the QG solution when $\partial v_g/\partial X = f$. Consistent with (4), one finds

$$g\frac{\theta'}{\theta_0} \approx f^2L^2/H \approx N_0{}^2H. \tag{14}$$

The corresponding PV anomaly, integrated over the infinitesimal layer in which it is concentrated, is

$$\frac{f\theta_0}{g}\left.\frac{\partial\psi'/\partial Z}{f^2-\partial^2\psi'/\partial X^2}\right|_{Z=0+}$$

$$= q_g\left.\frac{g\theta'/\theta_0}{N_0{}^2+(g/\theta_0)(\partial\theta'/\partial Z)}\right|_{Z=0+} \approx q_gH. \tag{15}$$

In the warm sector at the surface, and the cold sector at $Z = H$, this PV anomaly is positive. Diluted over the depth of the fluid, the PV should then increase by $\sim q_g$. Thus, the occluded air contains enough PV to increase the average value in the interior by an amount of order unity, sufficient to stabilize the flow and cause the disturbance to disperse and decay.

Since the potential vorticity in the SG model plays the same role as static stability in a QG model, a similar equilibration can be expected from a modified QG model in which the global static stability is allowed to vary. One can construct such a model in the spirit of Lorenz (1960), by allowing $N^2(z)$ in the QG equations to be time dependent. The crucial difference from the primitive equation model is that no front forms so that diffusive effects cannot play any role. The only meaningful way to change the global static stability is to relate the change with upward heat transport by the large-scale wave. The rate of change of stability is then determined by the equation

$$\frac{\partial}{\partial t}\frac{\partial}{\partial z}[\theta] = -\frac{\partial^2}{\partial z^2}[w\theta], \tag{16}$$

where brackets denote a zonal average. The quasi-geostrophic set is otherwise unmodified, and the perturbation streamfunction is again assumed to be independent of latitude, so that the thermodynamic equation, for example, takes the form

$$\frac{\partial}{\partial t}\frac{\partial\phi}{\partial z} + \bar{u}_g\frac{\partial}{\partial x}\frac{\partial\phi}{\partial z} - \Lambda\frac{\partial\phi}{\partial x} + w\left(\frac{g}{\theta_0}\frac{\partial}{\partial z}[\theta]\right) = 0, \tag{17}$$

where ϕ is a QG perturbation streamfunction. No attempt is made to provide a formal justification for this approximation. In fact, the detailed evolution predicted by this system is very different from that predicted by the primitive equations. Most importantly, there is still no wave–wave interaction; an initial disturbance consisting of one zonal harmonic never excites other harmonics, and no frontal formation is possible. The only nonlinearity is the static stability change (16) which then feeds back on the dynamics through the thermodynamic equation (17).

With the same initial condition as in the nongeostrophic control experiment, the wave enters a very similar life cycle. The evolution of the domain-averaged static stability of this system is compared with the control in Fig. 4. The maximum stability attained is close to, but slightly smaller, than in the control, and a qualitatively similar oscillation follows. The evolution of eddy kinetic energy is compared with the control in Fig. 9. This QG model with variable static stability appears to qualitatively capture the equilibration characteristics of the wave. Because horizontal scales do not change with time in this simplified system, we can apply scaling arguments to predict the equilibrated amplitude with greater confidence than for the full primitive equation solution. As before, we assume that there has to be an O(1) increase in N for the shift in the short-wave cutoff to stabilize the wave. The increase in global stability is a result of the upward heat flux, so we require

$$\delta N^2 \approx N_0{}^2 \approx -\frac{g}{\theta_0}\frac{\partial^2}{\partial z^2}\int_0^{t_0}[w\theta]dt. \tag{18}$$

Using standard quasi-geostrophic scaling,

$$\frac{\partial}{\partial z}\approx\frac{1}{H},\quad \frac{\partial}{\partial x}\approx\frac{1}{L},\quad \mathrm{O}\left(\frac{g}{\theta_0}\theta\right)\approx\frac{fL}{H}\mathrm{O}(v),$$

$$\mathrm{O}(w)\approx \mathrm{Ro}\,\frac{H}{L}\mathrm{O}(v),$$

where $\mathrm{Ro}\equiv\Lambda H/(fL)$, assuming a growing wave $|v| \approx |v_0|e^{t/\tau}$, with $\tau^{-1}\approx f\Lambda/N_0$, and ignoring factors of order unity, (18) reduces to

$$N_0{}^2 \approx |v_0|^2\frac{\tau f\,\mathrm{Ro}}{2H^2}(e^{2t_0/\tau}-1). \tag{19}$$

Further assuming that the final amplitude is much larger than the initial amplitude, and that $\mathrm{Ro}^2\,\mathrm{Ri} \approx \mathrm{O}(1)$, or equivalently $L \approx N_0H/f$, (19) becomes

$$N_0{}^2 \approx \frac{1}{H^2}|v_f|^2.$$

The predicted equilibrated amplitude is

$$|v_f| \approx N_0H,$$

identical with (13).

That the QG model without a front predicts the correct order of magnitude for the equilibrated amplitude implies that the characteristics of the front itself have little to do with the final amplitude of the wave, although mixing in the frontal region is necessary to trigger the equilibration in the full model.

Just as one can remove the frontal formation but retain the effects of the stability change, as in the QG

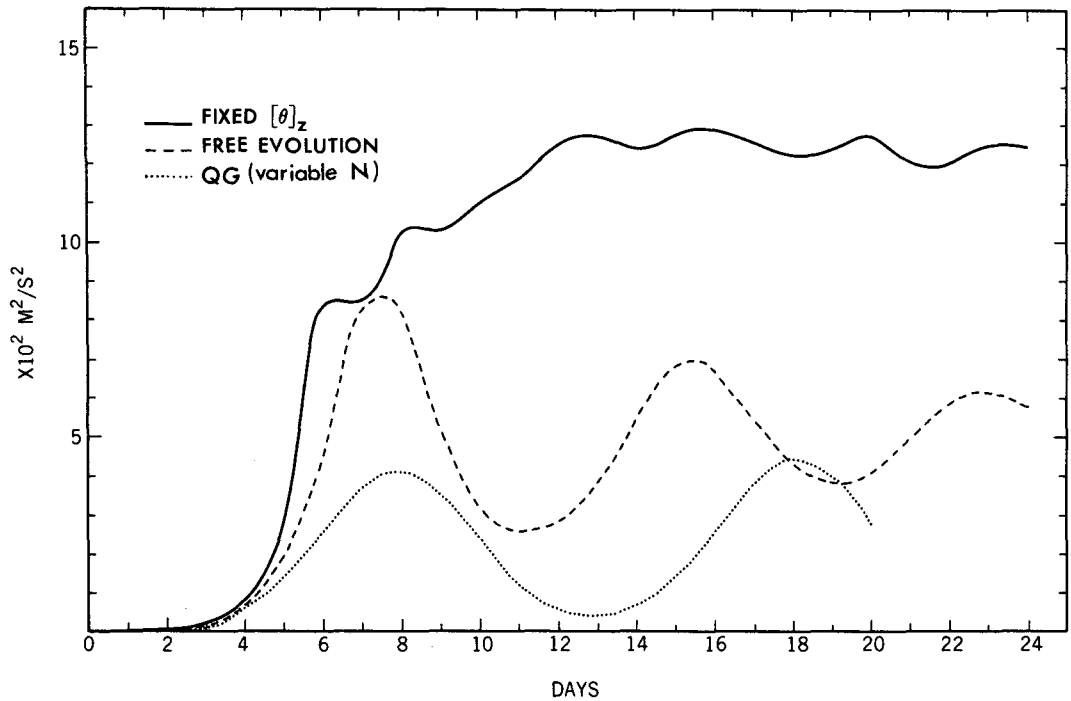

FIG. 9. Evolution of domain-averaged eddy kinetics energy. Dashed curve: Control. Solid curve: With a fixed zonal mean static stability. Dotted curve: QG with a variable zonal-mean static stability.

model with time-dependent N, one can try to retain the frontal formation but remove the effects of the stability change by simply fixing the horizontal mean of the potential temperature as a function of height. (One could also try to fix the mean interior potential vorticity, but this would be much more difficult to implement.) The result of such a calculation with the same initial condition as in the control, as well as the same resolution and diffusivities, is shown in Fig. 10. By day 6 the more violent frontal dynamics that arise are not well resolved. The evolution of the eddy kinetic energy is compared with that in the control and in the QG variable stability run in Fig. 9. The energy increases to considerably greater values than in the other two models. Inspection of the energetics shows that the baroclinic generation of kinetic energy does not halt; there is no change in sign of the vertical tilt. Rather, the direct destruction of eddy energy by diffusion, and by transfer to mean kinetic energy through the vertical momentum flux, increase in a complex way to balance the continuous baroclinic generation. While higher resolution seems to be needed to pass through the frontal collapse in a meaningful way when $N(z)$ is specified, given the small scale shear instabilities and gravity waves that seem to be generated, and while it is difficult to interpret the model in terms of PV dynamics, it is clear that the equilibration mechanism in this solution is very different from that in the calculations in which the static stability is free to vary.

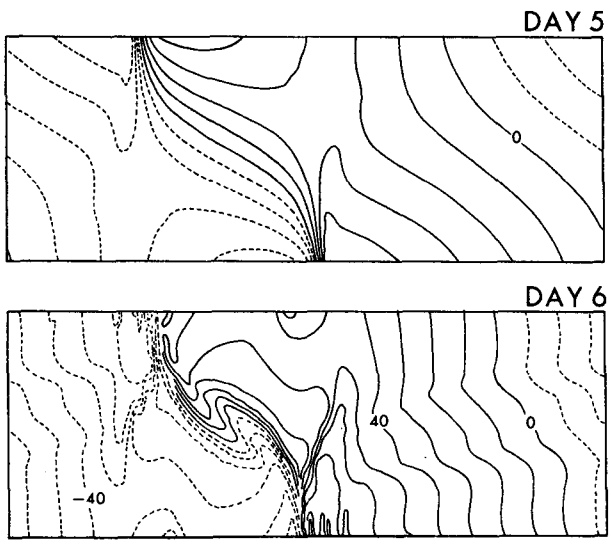

FIG. 10. Same as Fig. 2, but for the case with a fixed static stability.

4. Summary and discussion

We describe the evolution of an unstable Eady wave as it passes through the point of frontal collapse, reaches a maximum amplitude, and then decays. This equilibration is found to be caused by the increase in the potential vorticity in the frontal region. We think of this potential vorticity as being generated by transport from the boundary reservoir in the process of occlusion,

this process being made possible by diffusive mixing. (Without diffusion the front does collapse to the grid scale of the model.) Nevertheless, the maximum amplitude of the wave seems to be insensitive to the diffusivity and is solely determined by the parameters of the basic flow. A simple scaling argument yields the estimate $v \approx N_0 H$ for the amplitude that the wave attains. This cannot be the dominant mode of equilibration for large-scale disturbances in the atmosphere. The estimated amplitude, $N_0 H$, is much too large, and the large increases in potential vorticity (or static stability) that are responsible for the equilibration are unrealistic. It is much more reasonable to assume that large-scale disturbances equilibrate by modifying the horizontal temperature gradient, a mechanism eliminated by our unrealistic assumption of two-dimensional flow. If an unstable wave on an f-plane is instead assumed to generate a poleward eddy heat flux with the meridional scale L_y, then a scaling argument analogous to that in section 3 shows that the horizontal temperature gradient will be reduced by O(1) when the wave grows to the point that

$$|v_f| \approx L_y \frac{f\Lambda}{N_0}. \tag{20}$$

If the mode is isotropic, with $L_y \approx L \approx N_0 H/f$, this simply becomes

$$|v_f| \approx \Lambda H, \tag{21}$$

which is identical to the closure proposed by Stone (1972). The ratio of the amplitude predicted by the modification of potential vorticity to that predicted by modifying the horizontal temperature gradient is

$$\frac{L_x}{L_y} \mathrm{Ri}^{1/2}. \tag{22}$$

As long as Ri is large and the eddy is isotropic, the wave will equilibrate before it has a chance to increase the potential vorticity appreciably. Mesolows that form over the warm oceans in winter appear to be prime candidates for the equilibration mechanism discussed in this paper. To the extent that they are anisotropic, with $L_y > L_x$, this mechanism would be favored further over the alternative of stabilization by the horizontal heat flux. In reality, the horizontal inhomogeneity of the environment, and the possibility that normal modes do not have time to develop, complicates any attempt to relate these results to observed developing disturbances.

An interesting point arises concerning the relative timing of frontal formation and the equilibration of the large-scale disturbance. The two-dimensional Eady wave forms a front just prior to the leveling off of the amplitude. If waves in the atmosphere generally equilibrate by other mechanisms, by decreasing the horizontal gradient, or by spinning up to a large barotropic zonal flow as described by James (1987), then it seems that one should expect to see fronts forming only well after the equilibration of the large-scale disturbance. Since this is counter to observations, it is evidently dangerous to take the relative timing of frontal formation and equilibration from the two-dimensional model as indicative of this relationship in more realistic three-dimensional disturbances.

Acknowledgments. This work emerged largely from the authors' communication with Dr. I. Orlanski. We would like to thank Dr. B. Ross and Mr. L. Polinsky for the assistance in numerical modeling; Mr. Phil Tunison and his group for drafting the figures; and Ms. Sachi Kumon for typing the manuscript. Two anonymous readers' comments on the earlier version of the text are gratefully acknowledged. The first author's work has been supported by NSF Grant ATM821876A01.

REFERENCES

Arakawa, A., 1962: Non-geostrophic effects in the baroclinic prognostic equations. *Proceedings International Symposium Numerical Weather Prediction,* WMO, Tokyo, 161–175.

Bretherton, F. P., 1966: Critical layer instability in baroclinic flows. *Quart. J. Roy. Meteor. Soc.,* **92,** 335–345.

Charney, J. G., 1947: The dynamics of long waves in a baroclinic westerly current. *J. Meteor.,* **4,** 135–162.

Eady, E. T., 1949: Long waves and cyclone waves. *Tellus,* **1,** 33–52.

Gall, R. L., R. T. Williams and T. L. Clark, 1987: On the minimum scale of surface fronts. *J. Atmos. Sci.,* **44,** 2562–2574.

Garner, S. T., 1989: Fully Lagrangian numerical solutions of unbalanced frontogenesis and frontal collapse. *J. Atmos. Sci.,* **46,** 717–739.

Haynes, P. H., and M. E. McIntyre, 1987: On the evolution of vorticity and potential vorticity in the presence of diabatic heating and other forces. *J. Atmos. Sci.,* **44,** 828–841.

Hoskins, B. J., 1975: The geostrophic momentum approximation and the semi-geostrophic equations. *J. Atmos. Sci.,* **32,** 233–242.

——, and F. P. Bretherton, 1972: Atmospheric frontogenesis models: Mathematical formulation and solution. *J. Atmos. Sci.,* **29,** 11–37.

James, I. N., 1987: Suppression of baroclinic instability in horizontally sheared flows. *J. Atmos. Sci.,* **44,** 3710–3720.

Lorenz, E. N., 1960: Energy and numerical weather prediction. *Tellus,* **12,** 364–373.

Orlanski, I., 1986: Localized baroclinicity: A source for meso-α cyclones. *J. Atmos. Sci.,* **43,** 2857–2885.

——, and B. B. Ross, 1977: The circulation associated with a cold front. Part I: Dry case. *J. Atmos. Sci.,* **34,** 1619–1633.

Pedlosky, J., 1987: *Geophysical Fluid Dynamics.* Springer. 710 pp.

Simmons, A. J., and B. J. Hoskins, 1978: The life cycles of some nonlinear baroclinic waves. *J. Atmos. Sci.* **35,** 414–432.

Stone, P. H., 1972: A simplified radiative-dynamical model for the static stability of rotating atmospheres. *J. Atmos. Sci.,* **29,** 405–418.

Williams, R. T., 1967: Atmospheric frontogenesis: A numerical experiment. *J. Atmos. Sci.,* **24,** 627–641.

——, 1972: Quasi-geostrophic versus non-geostrophic frontogenesis. *J. Atmos. Sci.,* **29,** 3–10.